Polymer Testing 112 (2022) 107650

Contents lists available at ScienceDirect

Polymer Testing

journal homepage: www.elsevier.com/locate/polytest

On the temperature dependence of the cyclic compression behaviour of a thermoplastic vulcanizate elastomer

Anna-Maria M.R. Persson [a,b,*], Einar L. Hinrichsen [a], Erik Andreassen [a]

[a] SINTEF Industry, Polymer and Composite Materials Group, PO Box 124 Blindern, 0314, Oslo, Norway
[b] NTNU, Dept. of Manufacturing and Civil Engineering, PO Box 191, 2802, Gjøvik, Norway

ARTICLE INFO

Keywords:
Mullins effect
Compression set
Hysteresis loss
Thermoplastic elastomer
Bulk modulus
Poisson's ratio

ABSTRACT

Effects of temperature on the uniaxial cyclic compression of a polypropylene based thermoplastic vulcanizate were studied in the range −40 °C–100 °C. The effect of temperature on the stress level was similar to that on the storage modulus from dynamic mechanical analysis. The residual strain after a cycle increased with decreasing temperature below 23 °C, while from 23 °C to 100 °C the effect of temperature was small. Both dependencies were correlated with the effect of temperature on the fraction of stress relaxed in the cycle. The residual strain after a cycle and the standard compression set (ISO 815–1, method A) had different temperature dependencies, and this was rationalized based on the different timescales of the tests and the different temperatures during loading and unloading. Two different methods for determining the Poisson's ratio in this temperature range were investigated in terms of measurement accuracy. The preferred method was based on input from dynamic mechanical analysis and triaxial compression.

1. Introduction

Thermoplastic elastomers (TPEs) are used in an increasing quantity [1,2]. TPEs are soft and elastic to large strains [1,3]. Compared to crosslinked elastomers (rubbers), the advantages of TPEs include fast production processes, and good possibilities for material recycling [1,3], while the limitation of TPEs is the less ideal elastomeric behaviour, such as higher compression set, and a stronger temperature dependence of the properties [1,3].

Thermoplastic vulcanizates (TPVs) are a special type of TPEs, combining a crosslinked elastomer and a thermoplastic [1,2]. The morphology is phase separated; rubber particles are dispersed in a thermoplastic matrix, and the structure is created by dynamic vulcanization of melt mixed ingredients [1–4].

Several studies have related the mechanical behaviour of TPVs to the microstructure [5–11]. The review by Ning et al. [6] assessed effects of individual factors on the mechanical behaviour, but also remarked that the mechanisms behind the mechanical behaviour remain unclear.

Most commercial TPVs are based on polypropylene (PP) as the thermoplastic, and ethylene propylene diene monomer (EPDM) as the dispersed rubber [1,3], referred to as TPV-(EPDM + PP) materials. For improved properties, such as lower compression set at high temperatures, there are PP-based TPVs with other rubbers, such as cross-linked poly(styrene-b-(ethylene-r-butylene)-b-styrene) triblock copolymer (xSEBS). The type of rubber and thermoplastic, and the rubber fraction, are the main factors determining the TPV properties [1–4]. Some other important factors are (1) the chemical compatibility between the thermoplastic and rubber phases [12,13], (2) the crosslink density and network architecture [14,15] and (3) the details of the vulcanization and vulcanization agents [7,10,16,17].

The response to cyclic loading has been studied extensively for TPEs and rubbers. These elastomer materials exhibit effects such as Mullins effect [18], hysteresis, and an increase in residual strain and reduction in stress level for each loading cycle. These effects were first studied for particle filled rubbers, refer to the review by Diani et al. [19]. Drozdov and Dusunceli [20] performed tensile cycling of PP and noted similar effects on stress, residual strain and hysteresis loss. Most literature on cyclic loading of TPVs consider tensile loading at 23 °C, see Table 1, but there are also some studies of cyclic compressive loading: Wang et al. [21] studied cyclic compression of a TPV (crosslinked ethylene-vinyl acetate with styrene butadiene rubber) and evaluated the effect of strain amplitude on residual strain and hysteresis loss. Heat treatment of the specimens after testing (for 30 min) partially healed the Mullins effect (reduced the softening when re-testing) and partially recovered

* Corresponding author. SINTEF Industry, Polymer and Composite Materials Group, PO Box 124 Blindern, 0314, Oslo, Norway.,
E-mail addresses: anna-maria.persson@sintef.no (A.-M.M.R. Persson), einar.l.hinrichsen@sintef.no (E.L. Hinrichsen), erik.andreassen@sintef.no (E. Andreassen).

https://doi.org/10.1016/j.polymertesting.2022.107650
Received 7 July 2021; Received in revised form 4 May 2022; Accepted 24 May 2022
Available online 28 May 2022

the residual strain, and both effects increased with increasing heat treatment temperature [21]. Liu et al. [22] studied the effect of the rubber weight fraction for TPVs of HDPE and EPDM. Compared to 100% EPDM, the TPV exhibited significantly higher stress, and larger residual strain and hysteresis loss [22]. Also, the effect of an increased HDPE fraction was similar to the effect of an increased strain amplitude [22]. The literature on cyclic loading of TPVs/TPEs at other temperatures than 23 °C is limited. Drozdov and Christiansen [23–25] studied cyclic tensile loading of a TPE in the temperature range from 25 °C to 90 °C. The TPE was a carbon black reinforced hydrated styrene block copolymer [24]. They noted an effect of strain rate on the stress level, which was more pronounced at high temperature [24]. Neither strain rate nor temperature had a significant effect on the residual strain [24]. Material models for the response to cyclic loading are typically phenomenological [19]. Many of these models are generic and can be used for many types of polymer-based materials. The models usually include a combination of non-linear elasticity, viscoelasticity and viscoplasticity. Chagnon et al. [26] remarked that the Mullins effect may be realistically modelled as mechanical damage to the material, even though it is a stress softening phenomenon.

There are few published studies on the effect of temperature on the cyclic loading response of TPV materials. Also, there are few studies of cyclic compression compared to studies of cyclic tension, although for typical TPV applications, such as seals, the compressive properties are more important than the tensile properties.

This article investigates the cyclic compression behaviour of a TPV in a wide temperature range, focusing on the following key properties: Modulus, residual strain after unloading (compression set), hysteresis loss and Poisson's ratio. Furthermore, the instant compression set after a cycle is compared to results from the standard compression set test. This article also addresses methods for determining the Poisson's ratio. When modelling the mechanical behaviour of nearly incompressible [28] TPVs, using a correct Poisson's ratio is imperative.

The material in this study is a commercial TPV-(xSEBS + PP). This class of TPVs generally has lower compression set compared to the more common TPV-(EPDM + PP) materials. The TPV in this study has been the subject of other studies by the authors; one study comparing its cyclic compression response to that of three rubbers (two EPDMs and one LSR) [29], and one study on the TPV's adhesion to hard polyamide materials in two-component injection moulding [30].

2. Experimental

2.1. Material and specimen preparation

The TPV in this study is a commercial material; Thermolast TV6VAZ from Kraiburg (Waldkraiburg, Germany). This TPV is based on cross-linked SEBS in a PP matrix, referred to as TPV-(xSEBS + PP). The hardness of the TPV is Shore A 60, and it is modified for improved adhesion to polyamides. Note that TPV-(xSEBS + PP) materials without this modification typically have lower compression set.

TPV plates with thicknesses 2.0, 3.4 and 4.0 mm were injection moulded (IM). The processing temperature was chosen from the higher end of the processing window suggested by the material producer. The injection speed was set to have the same flow front speed in the plates as in IM standard tensile test specimens (type 1A of ISO 527–2) in accordance with ISO 294–1.

An EPDM rubber with hardness Shore A 60 (compound E6T30), in the form of compression moulded plates, was purchased from Trelleborg Sealing Solutions.

2.2. Thermo-mechanical characterization

Differential scanning calorimetry (DSC) was performed with a TA Instruments DSC2500 instrument. A 3.3 mg sample was cut from an IM plate and placed in aluminium pan. The sample was heated, cooled and heated again, in the range −90 °C–200 °C (rate: 20 °C/min).

Dynamical mechanical thermal analysis (DMTA) was performed with a torsion fixture in an Anton Paar MCR 502 rheometer. The specimen dimensions were 50 × 10 × 3.4 mm^3, stamped from 3.4 mm thick IM plates. The temperature range was from −100 °C to 140 °C (rate: 1 °C/min), and the sinusoidal shear strain had an amplitude of 0.05% and a frequency of 1 Hz.

2.3. Cyclic uniaxial compression tests

Cylindrical specimens with diameter 11.4 mm were stamped from IM plates (2.5 or 4.0 mm thick). The specimen configuration was pre-studied (details not included here), to achieve uniaxial compression, i.e. minimized barrelling and having a uniform strain field over the specimen. A stack of three 4 mm thick cylinders led to an unstable stack (uneven strain field), and a single 2.5 mm layer experienced barrelling. The other combinations gave similar and satisfactory strain fields. The standard configuration was chosen to be a stack of two 4 mm thick cylinders, i.e. the specimen was a cylinder with height 8 mm and diameter 11.4 mm (aspect ratio 0.70). In the standard for compressive testing of elastomers (ISO 7743), test piece A has aspect ratio 0.42, and test piece B aspect ratio 1.40. The roughness of the top and bottom specimen surfaces was given by the polished IM tool surface.

Cyclic uniaxial compression tests were performed with a universal testing machine (Zwick Z250). The cylindrical specimens were lubricated with a mineral oil-based grease (Molykote BR2 Plus) in order to

Table 1
Cyclic loading studies of TPVs.

Thermoplastic	Rubber	Weight fractions	Res. strain 1st cycle (max strain)	Maximum strain in cycle	Test details	Ref.
HDPE	EPDM	20–80	~9% (50%)	10–50% stepwise	Compression, 23 °C	[22]
PP	EPDM	50–50	28% (100%)	100% (+stepwise)	Tension, 23 °C	[27]
PA6	EPDM	40–60	~54% (100%)	100% SC	Tension, 23 °C	[11]
PA6	XHNBR& HNBR	40-42-18	~58% (100%)	10–100% stepwise	Tension, 23 °C	[14]
HIPS, SBS[a]	SBR	30-9-70	~13% (50%) ~30% (100%)	50–250% stepwise	Tension, 23 °C	[12]
EVA	SBR (CB)	30-70(-30)	~2.5 (10%) ~17% (50%)	10–50% stepwise	Compression, 23 °C	[21]

CB: Carbon black.
HIPS: High impact polystyrene.
Res strain: Residual strain after cycle.
SBR: Styrene butadiene rubber.
SBS: Styrene butadiene styrene copolymer.
Stepwise: Repeated cycles to larger strains with the same sample.
SC: Single cycle.
[a] Compatibilizer.

minimize the friction towards the steel plates of the compression fixture. The tests were performed at five temperatures from −40 °C to 100 °C, and non-room temperature tests were performed in a temperature chamber. For the first loading cycle at −40 °C, stress build up was delayed, which could be due to thickening of the grease and too low pre-force. The temperatures in the chamber, and in a dummy specimen with a thermocouple, were logged in most experiments, to ensure stabilized temperature in the specimen prior to testing.

Eight compressive loading-unloading cycles were applied, between a low pre-force and a strain amplitude of 25%, with a 2 s hold period between each change of deformation direction. The tests were repeated (with new specimens) minimum three times at each temperature. Tests to higher strain amplitudes were also performed (40–50% and 70%) at 23 °C and 100 °C. The crosshead speed for the specimen with height 8.0 mm (stack of two discs) was 6.4 mm/min.

For most tests, the strain field was measured optically with 3D digital image correlation (DIC). The black specimens were prepared for DIC measurements by applying a fine white speckle pattern (Fig. 1b). A white base coat was also tested, for possibly improving the DIC measurements, Fig. 1c. However, the white coat was problematic, at both low and high test temperatures, due to cracking or detachment. The optical measurements at sub-zero temperatures were not successful, due to ice crystals appearing on the surface of the specimen. The DIC system was VIC 3D from Correlated Solutions. Two cameras with resolution 2452 × 2052 and 75mm/f2.8 lenses were used. The setup is depicted in Fig. 1a. The two cameras were mounted side by side, in order to have a clear view of the specimen which was positioned between compression plates having a larger diameter than the specimen. The entire cylindrical specimen could not be in focus, and the focus was set at the centre of the specimen (aperture f8 was used).

Under the assumption that the deformation of the lubricated cylindrical specimen is uniaxial and uniform (specimens exhibiting clear barrelling were excluded based on the optical recording), this setup allows for measuring the strains, in order to estimate the Poisson's ratio. The Poisson's ratio (ν) was calculated from the axial and circumferential strains (ε_z and ε_θ) according to Eq. (1).

$$\nu = -\varepsilon_\theta/\varepsilon_z \tag{1}$$

Hencky strains were used in Eq. (1), while nominal stresses and strains were used in Eqs. (2)–(5). For the loading of cycle (n), a secant modulus ($S_{25\%,n}$) was calculated from Eq. (2) using the maximum stress $\sigma_{max,n}$ and the corresponding strain $\varepsilon_{max,n}$, see Fig. 2. Note that, for all cycles, this secant modulus is the slope from the origin, i.e. the start of the first loading cycle. Hence, it is the secant modulus relative to the specimen height prior to testing.

$$S_{25\%,\,n} = \sigma_{max,\,n}/\varepsilon_{max,\,n} \tag{2}$$

A cyclic compression set after a given cycle CCS_n, i.e. the strain set after unloading to the small pre-force in cycle n, was calculated from Eq. (3), based on the maximum strain before unloading ($\varepsilon_{max,n}$, typically 25%) and the residual strain after unloading ($\varepsilon_{res,n}$), see Fig. 2.

$$CCS_n = \varepsilon_{res,\,n}/\varepsilon_{max,\,n} \tag{3}$$

The hysteresis loss in cycle n (U_n), i.e. the energy dissipated in load

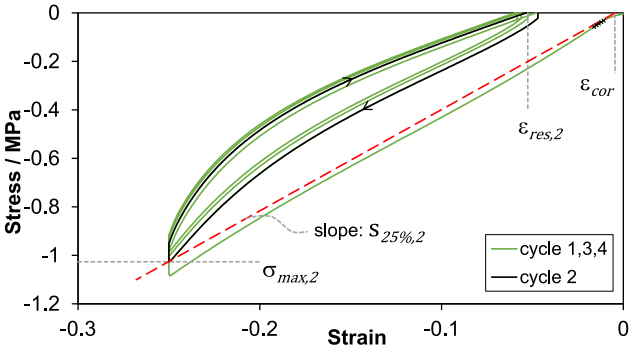

Fig. 2. Example of experimental data for cyclic loading to 25% compressive strain, and some characteristics for the 2nd cycle; maximum stress after 2nd loading ($\sigma_{max,2}$), residual strain after 2nd unloading ($\varepsilon_{res,2}$), and the secant modulus of the 2nd loading curve relative to the original specimen height ($S_{25\%,2}$). In some tests, the first loading curve did not pass through the origin due to too small pre-stress. In these cases, the strains were corrected with a correction strain (ε_{cor}), which was obtained by fitting a linear function (not shown) to the experimental curve in the interval 0.03–0.06 MPa (marked with x symbols in the figure).

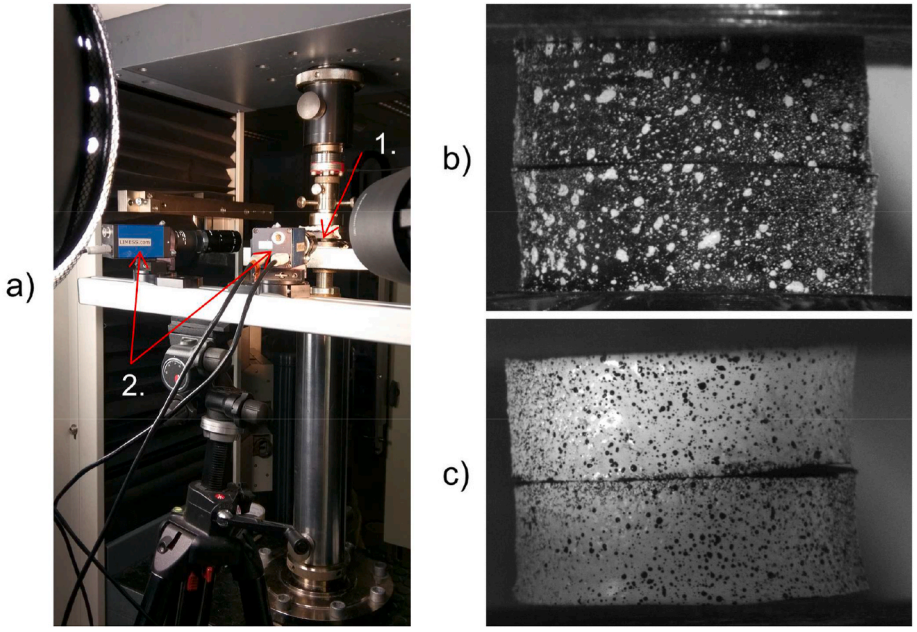

Fig. 1. a) Experimental setup. 1: The specimen between compression plates. 2: The two DIC cameras. b) DIC paint speckle pattern; white paint droplets on the black TPV. c) As b), but black droplets on white base coat.

cycle n, was calculated from the area of the nth loading-unloading loop (Eq. (4)). A relative hysteresis loss ($U_{rel,n}$) was calculated by dividing the absolute loss with the area under the loading curve (Eq. (5)).

$$U_n = \oint_n \sigma d\varepsilon \tag{4}$$

$$U_{rel,n} = U_n \Big/ \int_{\varepsilon_{min,\ n}}^{\varepsilon_{max,\ n}} \sigma d\varepsilon \tag{5}$$

2.4. Triaxial compression tests

Triaxial compression tests were performed with a specimen placed inside a cylinder and loaded with a piston. The specimen was lubricated the same grease as in the uniaxial tests. The diameter of the cylinder and specimen was 25 mm, and the specimen height was 8 mm (a stack of two disks). 10% strain (axial and volumetric) was applied with a crosshead speed of 1 mm/min. The initial stiffness (referred to as k) was calculated between 2 and 5% strain. The strain was applied for 1 h before unloading. Directly after unloading, the volumetric compression set was measured (at the test temperature).

For this test, if we assume zero transversal strain in the cylindrical specimen, an isotropic linear-elastic material law gives the following relation between the axial stress (σ_z) and the transversal stress ($\sigma_r = \sigma_\theta$):

$$\sigma_r = \frac{\nu}{1-\nu}\sigma_z \tag{6}$$

The relation between axial stress and axial strain can be written as:

$$\sigma_z = 3K\frac{(1-\nu)}{(1+\nu)}\varepsilon_z = k\varepsilon_z \tag{7}$$

where K is the bulk modulus and k is the initial slope of the stress-strain curve. Hence, for an incompressible material ($\nu = 0.5$), the stress in the specimen is hydrostatic ($\sigma_z = \sigma_r$) and the bulk modulus can be obtained directly from the initial slope ($k = K$) (assuming that the material is linear-elastic initially):

$$\sigma_z = K\varepsilon_z \tag{8}$$

The linear-elastic material parameters K, G and ν are related as:

$$K = \frac{2G(1+\nu)}{3(1-2\nu)} \tag{9}$$

By combining Eqs. (9) and (7), the Poisson's ratio can be expressed as a function of k and G:

$$\nu = \frac{2G-k}{2(G-k)} \tag{10}$$

With Eq. (10) the Poisson's ratio can be determined from the triaxial compression test in combination with G′ from DMTA. From this, the bulk modulus can be determined from Eq. (9) via Eq. (10).

2.5. Standard compression set tests

Compression set (CS) was tested at different temperatures based on the standard ISO 815–1, method A (25% compression, specimen height measurements at room temperature). The tests were repeated at least three times. The specimen configuration was a stack of two 4 mm thick discs with diameter 11.4 mm.

3. Results

3.1. DSC and DMTA

The DSC thermogram of the TPV shows a melting peak at 147 °C for the second heating, see Fig. 3 and a crystallization peak at 111 °C (not shown). These peaks are associated with the PP phase of the TPV material. The heat of fusion for the second heating was 17.0 J/g. The indication of a T_g at −53 °C, and an endotherm around 15 °C, are attributed to the SEBS [31].

The DMTA data (Fig. 4) shows a glass transition temperature (T_g) at −58 °C. The shear storage modulus decreases gradually with increasing temperature, from the T_g to the upper temperature of the measurements (125 °C). At −40 °C and 100 °C, the storage shear moduli are 17 and 1.8 MPa, respectively.

3.2. Cyclic uniaxial compression

3.2.1. Stress-strain curve shapes

Fig. 5a shows the first and second cycle, at temperatures from 23 °C to 100 °C. The temperature affects the loading as well as the unloading. The maximum stress decreases with increasing temperature. Fig. 5b shows the first and second cycle from −40 °C to 23 °C. The −40 °C experiment stands out with a more non-linear unloading curve and a higher residual strain. For all temperatures, the loading curve changes shape from the first cycle to the second (Fig. 5a and b). The difference between the second and 8th cycle is a moderate offset (Fig. 5c and d). For the second and 8th cycles (Fig. 5c and d), as the temperature decreases, the loading curve gets a more distinct S-shape and the unloading curve becomes more non-linear.

Curves for normalized stress vs. strain for the first cycle are shown in Fig. 6. The difference between normalized stress during loading and unloading is largest at the lowest temperature.

Stress-strain curves for higher strain amplitudes (40/50 and 70%) are shown in Fig. 7a and Fig. 7b, for tests at 100 °C and 23 °C, respectively. The qualitative effect of temperature is the same as for 25% strain. During loading, but especially during unloading, the non-linearity is more pronounced at 23 °C than at 100 °C. To further examine this, the derivatives of the loading and unloading curves are shown in Fig. 7c. For the loading to 70%, the derivative is higher for the 23 °C data than for the 100 °C data. The second derivatives are similar initially (equidistant derivative curves), but they start deviating for strains above ca 55%. For the unloading, the derivative is consistently higher at 23 °C, and, when comparing the two temperatures, the second derivatives mainly differ at large strains.

3.2.2. Modulus, cyclic compression set and hysteresis loss

The effects of temperature on the cyclic response are reported in the section, with the parameters defined in Eqs. (2)–(5). The secant modulus for the first loading ($S_{25\%,1}$) (Eq. (2)), shown in Fig. 8a, decreases with increasing temperature. At the lowest temperature (- 40 °C), the $S_{25\%,1}$ value is above the indicated trend for the other data points (dashed black line). The temperature dependence of $S_{25\%,1}$ is similar to that of G′ from the DMTA. The secant modulus for the 8th loading ($S_{25\%,8}$) is lower than

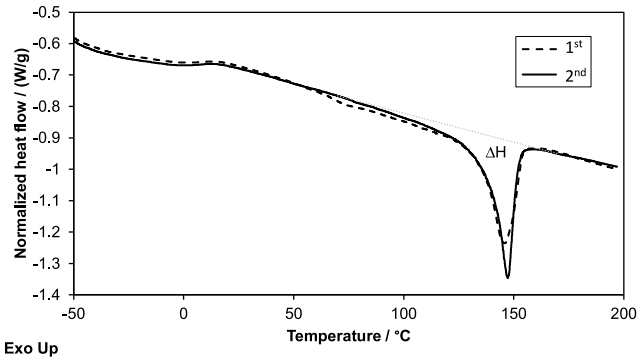

Fig. 3. DSC results for first and second heating.

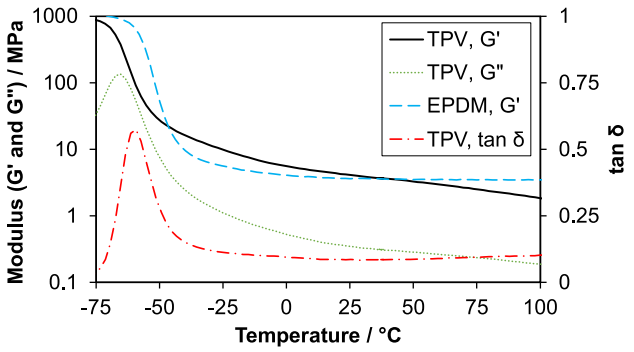

Fig. 4. DMTA results (cooling). Shear storage and loss moduli on the left axis. Loss factor on the right axis. The shear storage modulus of an EPDM rubber is included for the discussion.

$S_{25\%,1}$, but it has similar temperature dependence.

The cyclic compression set, CCS (Eq. (3)), shown in Fig. 8b, decreases with increasing temperature up to 23 °C, whereas from 23 °C to 100 °C it seems to reach a plateau. The CCS values are higher after the 8th unloading than after the 1st unloading, but the temperature dependence is the same.

The hysteresis loss, U (Eq. (4)), is shown in Fig. 8c. It decreases with increasing temperature, and the temperature dependence is similar to that of $S_{25\%}$ and G'. The relative loss, U_{rel} (Eq. (5)), is shown in Fig. 8d. U_{rel} is largest at −40 °C. There is no clear temperature dependence in the interval −10 °C–100 °C.

The evolution of the main parameters as function of cycle number is shown in Fig. 9. The secant modulus ($S_{25\%}$) vs. cycle number (Fig. 9a) follows a power law, as does the cyclic compression set (Fig. 9b). The hysteresis loss (Fig. 9c) and the relative hysteresis loss (Fig. 9d) both decrease with increasing cycle number. The reduction from one cycle to another is largest from the 1st to the 2nd cycle. From the 2nd cycle, both parameters follow a power law.

3.2.3. Poisson's ratio

Fig. 10a shows circumferential strain versus axial strain in cyclic compression. A small hysteresis between loading and unloading is observed. There is some scatter between the two tests shown. Fig. 10b shows (fits of) data for the first loading at 23, 60 and 100 °C. Up to at least 20% strain the Poisson's ratio is close at 0.5 at all temperatures. The Poisson's ratio determined from the slope of the quadratic fits in Fig. 10a and similar for the other temperatures, were 0.50 ± 0.03, 0.52 ± 0.02 and 0.49 ± 0.04 at 23, 60 and 100 °C respectively.

For comparison, Fig. 10c shows transverse versus axial strain in tension (only for loading). The dashed lines in Fig. 10b and c, representing Poisson's ratios of 0.5 and 0.4, respectively, indicate that the Poisson's ratio is larger in compression than in tension.

3.3. Standard compression set test

Standard compression set (CS) measurements (ISO 815–1, method A) were also performed. Effects of test time and test temperature are shown in Fig. 11a. At 100 °C, the CS value increases with test time up to about

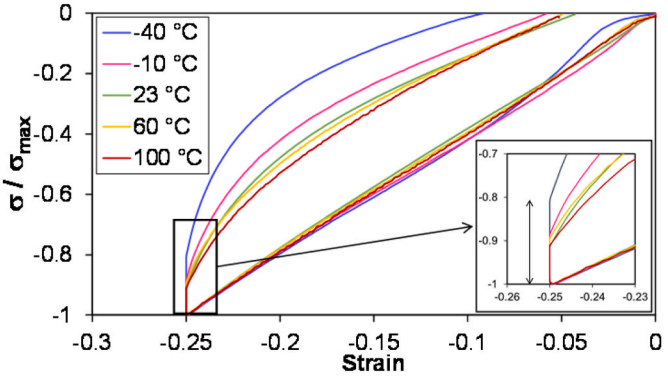

Fig. 6. Cyclic loading to 25% strain at various temperatures. Normalized stress versus strain for the first cycle. (The initial part of the curve at −40 °C is commented in Sect. 2.3.) The inset is a magnified view showing the stress relaxation occurring in the 2 s hold time after reaching the maximum strain.

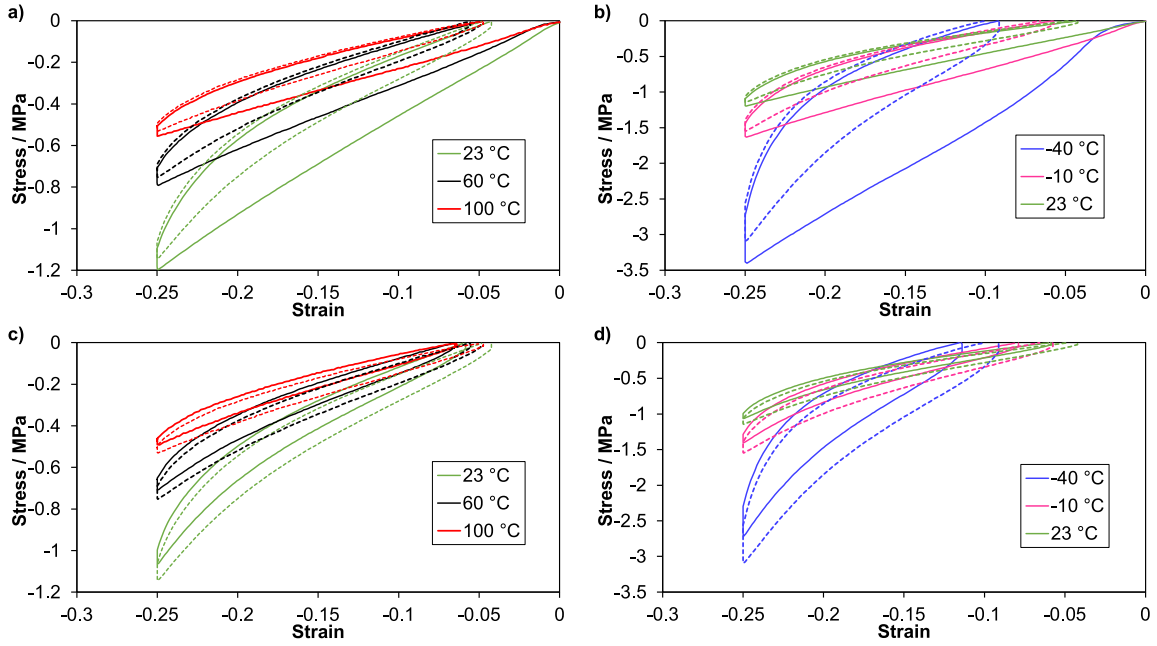

Fig. 5. Cyclic loading at various temperatures (see legends). Stress versus strain for a, b) first cycle (solid line) and 2nd cycle (dashed line), and c, d) 2nd cycle (dashed line) and 8th cycle (solid line).

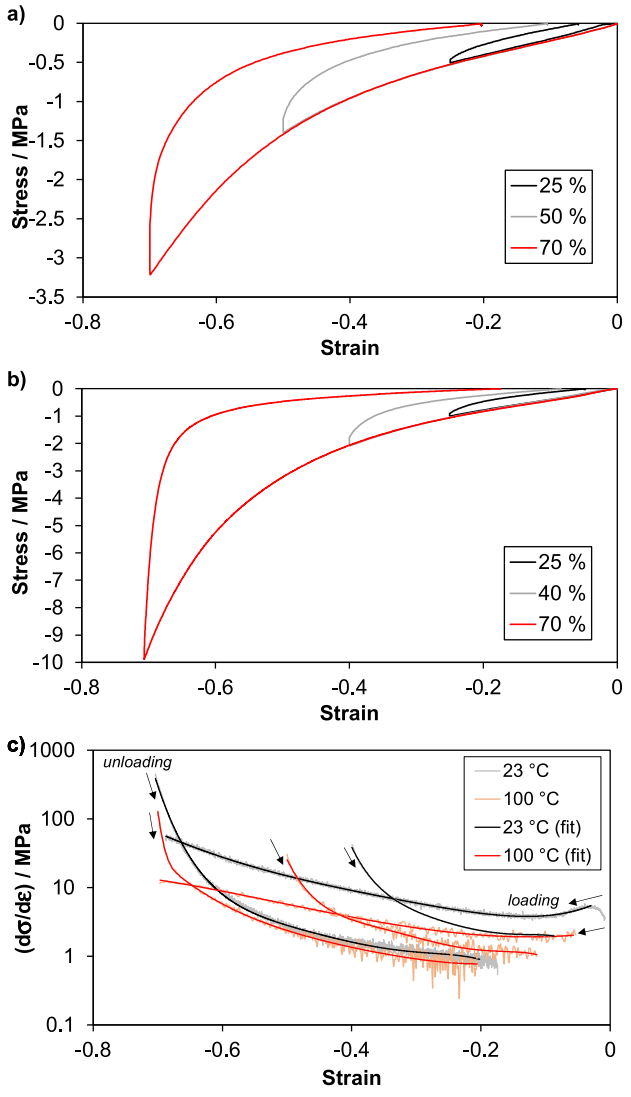

Fig. 7. Stress versus strain for uniaxial compression tests at a) 100 °C and b) 23 °C. Data for first loading and unloading, for different strains at unloading (one specimen per curve shown). c) Derivatives of the stress-strain curves in a) and b). Thick red and black lines indicate trends (fits), and thin lines are the calculated derivatives. (For interpretation of the references to colour in this figure legend, the reader is referred to the Web version of this article.)

350 h, and then levels off at about 63%. The CS value after 504 h (3 weeks) increases with increasing temperature, see also Fig. 11b.

3.4. Triaxial compression

The triaxial compression tests had a semi-long hold time (1 h) with constant displacement between loading and unloading. Hence, the results can be assessed either as a cyclic stress-strain curve (Fig. 12a) or as stress relaxation vs. time (Fig. 12b). The temperature has no clear effect on the relaxation rate (Fig. 12a and b). The relaxation rates are low, compared to typical values in uniaxial compression [32].

The bulk modulus can be assessed from these tests. If the Poisson's ratio is 0.5, the bulk modulus is equal to the initial slope (Eq. (8)), as plotted in Fig. 12c. The temperature affects the initial slope and to some extent the relaxation behaviour (Fig. 12b). The temperature also has a small effect on the unloading curve, and on the hysteresis area which is largest at 100 °C (Fig. 12a). The volumetric compression set, based on the instant residual volumetric strain after unloading (Fig. 12c), decreases with increasing test temperature; from 14% at −40 °C to 7% at 100 °C.

With the shear modulus from the DMTA measurements and the initial slope from the triaxial compression test, the Poisson's ratio can be estimated using Eq. (10). This gives Poisson's ratio values of 0.490; 0.497 and 0.499 at −40 °C, 23 °C and 100 °C, respectively. (Standard deviations are omitted since the DMTA was only repeated twice.) With these values, Eq. (9) allows for estimating bulk moduli, which are plotted in Fig. 12c.

4. Discussion

Since temperature effects is a key element in this paper, the first section below (Sect. 4.1) discusses the thermal characterization results. Then, Sect. 4.2 discusses the effects of temperature, cycle number and strain amplitude on the cyclic compression response; with sub-sections for each key property. Sect. 4.3 presents a microstructural deformation mechanism first proposed by Soliman et al. [33], and uses it as a tool in the discussion of temperature effects. Sect. 4.4 discusses the cyclic compression set (CCS) values vs. standard compression set values. Finally, the Poisson's ratios are discussed in Sect. 4.5.

4.1. DSC and DMTA

The measured heat of fusion can be used to estimate the PP fraction in our TPV. Wu et al. [34] studied a TPV-(xSEBS + PP + oil) with 20 wt% PP. The T_m of their TPV was about 153 °C (compared to 147 °C for our TPV). They reported a crystallinity degree of the PP phase of around 35%. If we assume that the PP in our TPV has a similar crystallinity as that in Ref. [34], then our measured heat of fusion corresponds to a PP fraction of about 24 wt%.

Our storage modulus (Fig. 4) is comparable to that in Ref. [35] for a TPV-(SBR + PP) with weight fractions 1:1. Our T_g at −58 °C (from tan δ, Fig. 4) corresponds to the soft segments of SEBS; ref. [36] observed a T_g around −55 °C for PP-SEBS blends. A T_g associated with amorphous PP was not seen in Fig. 4, unlike reports for a TPV-(SBR + PP) [35] where a small peak at 8 °C was assigned to the PP phase. The lower limit for the use of a TPV is related the elastomer T_g [3], but the T_g of the thermoplastic is also a governing factor.

4.2. Cyclic uniaxial compression

4.2.1. Effect of temperature on the modulus

The secant modulus ($S_{25\%}$) for the first loading (Fig. 8a) decreases with increasing temperature, with a temperature dependence similar to that of the shear storage modulus G' (Fig. 8a).

In the range −10 °C to 100 °C (Fig. 8a), the slope for the $S_{25\%}$ data appears to be slightly less steep than that of G′, especially at the highest temperatures. This is probably related to the different strain amplitudes; 25% in the cyclic compression test vs. 0.05% in the DMTA. It is expected that the relative effect of the rubber phase on the apparent stiffness increases with increasing strain. Hence, since the rubber stiffness is less sensitive to temperature than the PP phase, $S_{25\%}$ will be less sensitive to temperature than G'.

In Fig. 8a, the $S_{25\%}$ and G′ values are of similar magnitude. However, for a linear-elastic isotropic material, the tensile modulus (E) is up to three times larger than the shear modulus (depending on the Poisson's ratio). The low magnitude of $S_{25\%}$ compared to G′ is probably mainly related to the higher strain amplitude in the former test, but the lower strain rate can also play a role. We also considered if anisotropy in the injection moulded specimen could be a factor. The uniaxial compression strain is in the thickness direction of the injection moulded plate, while the DMTA shear strain was in the in-plane direction. However, the reported anisotropy of injection moulded PP-based TPVs [37] would contribute in the opposite direction of our observed effect.

The stress-strain curve for the second loading is affected by temperature: At 100 °C it is nearly linear, but for decreasing temperatures

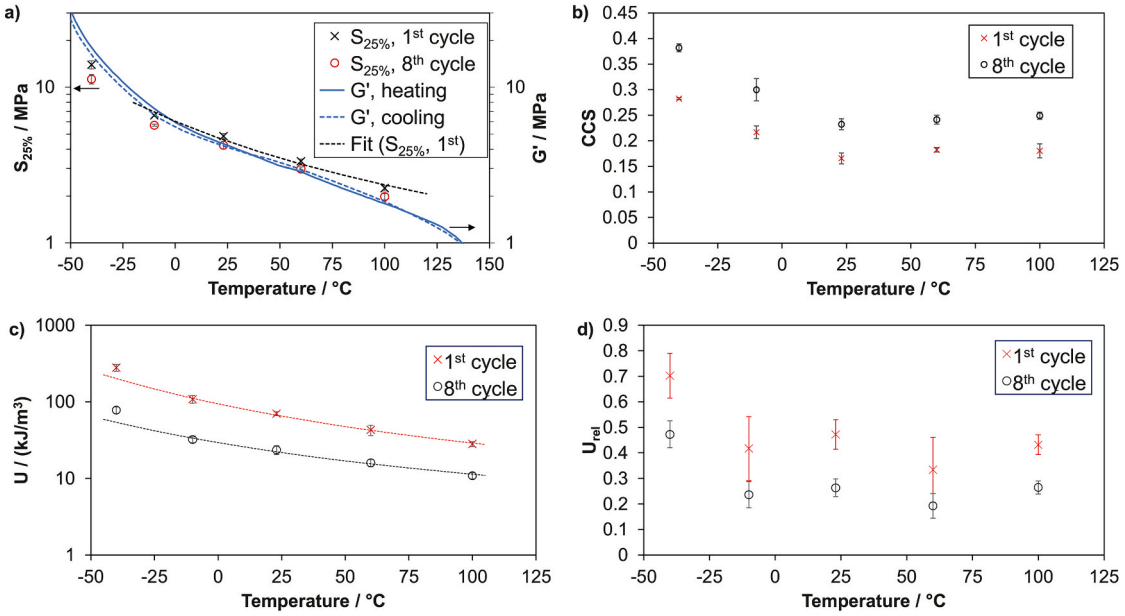

Fig. 8. Effect of temperature on three key properties. a) Secant modulus (dashed line represents an Arrhenius fit) and shear storage modulus. b) Cyclic compression set. c) Hysteresis loss (dashed lines are Arrhenius fits). d) Relative hysteresis loss.

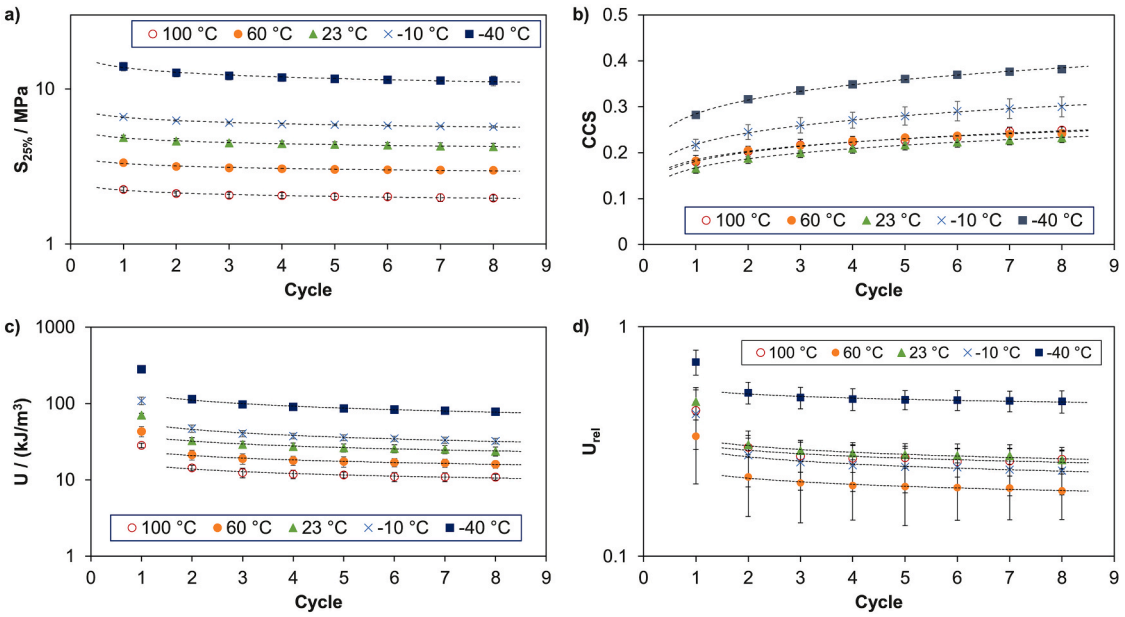

Fig. 9. Trends vs. cycle number: a) secant modulus, b) cyclic compression set, c) hysteresis loss and d) relative hysteresis loss. As guides for the eye, power law fits are shown as dashed lines.

the shape is increasingly non-linear, see dashed curves in Fig. 5ab and Fig. 6b. The difference between the first and second loading is due to the Mullins effect.

4.2.2. Effect of temperature on the cyclic compression set

The CCS data (Fig. 8b) shows two regimes of temperature dependence. 1) At 23 °C and above, the temperature has almost no effect. 2) Below 23 °C, a decrease in temperature leads to an increase in the CCS value. The regime with marginal temperature influence is similar to data published by Drozdov et al. [23–25], who studied the effect of temperature on the tensile cyclic response for a carbon black reinforced TPE, in the temperature range 20 °C–90 °C.

The small effect of temperature on the CCS value in the range 23 °C–100 °C seems to be related to the (small) temperature dependence of the relaxation of normalized stress, in the timeframe of a cycle. Fig. 6 shows that, in this temperature range, there is almost no effect of temperature on the normalized stress relaxation during the short hold period at 25% before unloading. Hence, the CCS value seems to be governed by the fraction of stress relaxed in the cycle; when this fraction is almost the same at a higher temperature, the CCS value will also be similar. In stress relaxation tests of the same TPV [32], the relaxation rates are almost the same at 23 °C and 100 °C, for the normalized stress during the first 1 h. This agrees with our conjecture above.

The temperature dependence of the stress relaxation of a PP

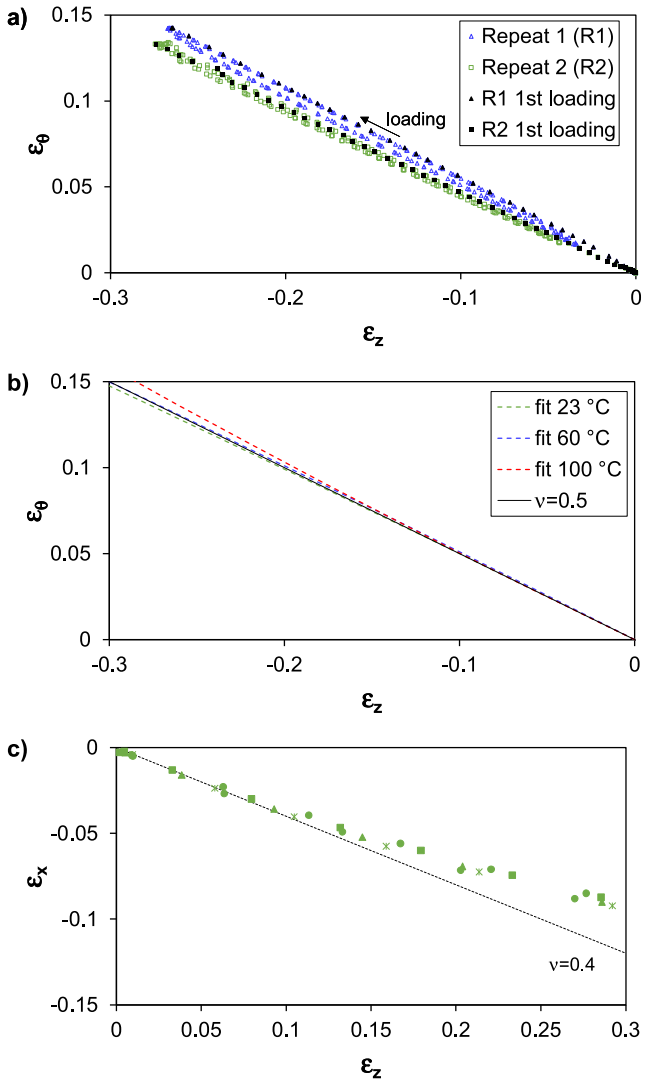

Fig. 10. Transverse strain versus axial strain from DIC measurements. Hencky strains are used in these diagrams. Dashed lines represent Poisson's ratios as indicated. a) Data for two cyclic compression tests, in blue and green, four cycles for each. Black symbols: Data used for quadratic fits. Note the variation between repeats. b) Quadratic fits of the first loading at three temperatures. The symbols are the average of fits of 2–4 repeats. (Some repeats shown with black symbols in diagram a). c) Data for loading in tension (five repeats). (For interpretation of the references to colour in this figure legend, the reader is referred to the Web version of this article.)

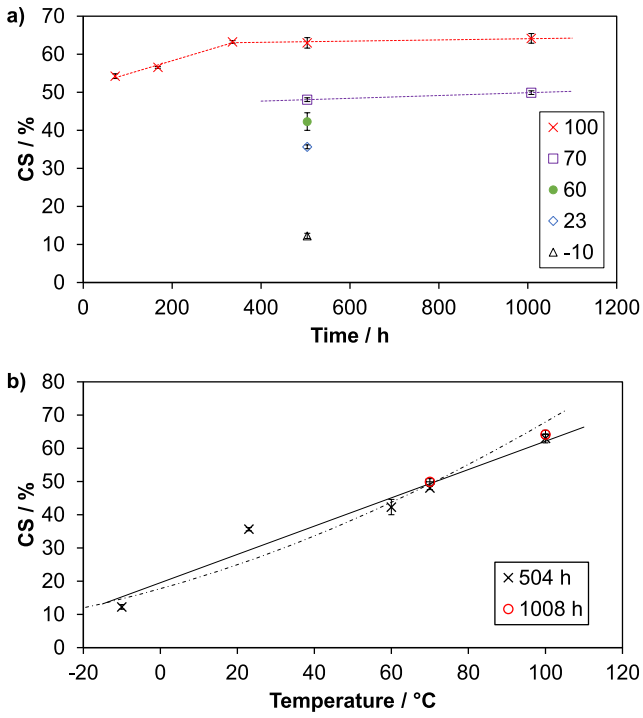

Fig. 11. a) Compression set versus test duration (legend: test temperature). b) Compression set versus test temperature (legend: test duration). The solid line is a linear fit of the 504 h data, and the dashed line is an Arrhenius fit (with activation energy E_a = 11.4 kJ/mol•K).

copolymer was published by Drozdov [38]. The PP phase will reach a stress plateau earlier at 100 °C than at 23 °C, as expected from time-temperature superposition of polymers that are more or less thermo-rheologically simple. This is not reflected in our CCS values, partly due to the dominant role of the elastomer phase, and partly due to the timeframe of our experiment.

For our CCS data at 23 °C, −10 °C and −40 °C, we observe an increase with decreasing temperature (Fig. 8b). Again, this seems to be related to the relaxation of normalized stress. At a lower temperature, the relaxation is higher (Fig. 6), causing a higher CCS value. However, below the T_g of the PP phase (not seen in the DMTA data, though), the mechanism is probably somewhat different from the case discussed above, since the hardness and possible damage of the PP may play a role. Stress relaxation tests of our TPV [32] show a similar temperature dependence in this temperature range. Initially (time <1 min), the normalized stress relaxes faster at −10 °C than at 23 °C. After this, the relaxation rates are similar (the data set ends at 1 h), but the degree of relaxation remains highest at −10 °C.

4.2.3. *Effect of temperature on the hysteresis loss*

The hysteresis loss (U) decreases with increasing temperature (Fig. 8c), and in the interval −10 °C–100 °C the temperature effect can be fitted with an Arrhenius function. In the same interval, the relative loss (U_{rel}) is nearly unaffected by temperature. At −40 °C, both U and U_{rel} are higher than the trend for the other temperatures. A large hysteresis loss may generate excessive heat, which is unwanted [3]. The relative loss characterizes the deviation from an ideal elastomer, which has zero loss.

4.2.4. *Trends vs. cycle number*

The main features of the stress-strain response for cyclic loading are generic for polymeric materials; for each new cycle there is a stress softening, a shift of the loading-unloading curve towards larger strains, and a reduction in the hysteresis loss [18,19]. There is a large difference between the first and second loading (also without a Mullins effect). After a certain number of cycles (e.g. 10), the difference between consecutive cycles is small.

The $S_{25\%}$ value decreases with increasing cycle number, following a power law (Fig. 9a). A similar softening behaviour has been reported for TPV-(EPDM + PP) [39], TPU [40] and TPV-(EPDM + HDPE) [22]. The CCS value increases with increasing cycle number, also following a power law trend (Fig. 9b). A similar trend has been reported for other TPEs [22,23].

Hence, $S_{25\%}$ and CCS values change gradually as function of cycle number, with no special transition between the first and second cycle, as for parameters affected by the Mullins effect. Note that our secant modulus (Eq. (2)) is really just representing the stress at 25% strain.

The U value decreases with increasing cycle number (Fig. 9c). A larger reduction is seen from the 1st to the 2nd cycle than between the other cycles. This is due to the Mullins effect. From the 2nd to the 8th

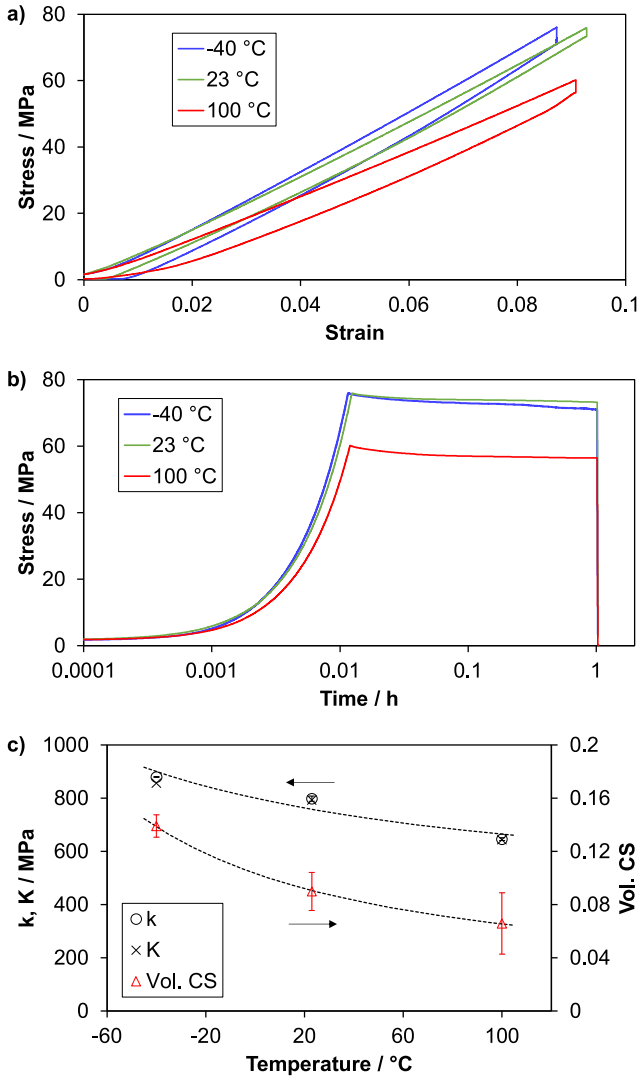

Fig. 12. Triaxial compression results at −40, 23 and 100 °C. a) Stress versus strain (the curves are horizontally shifted so that zero strain corresponds to 1.6 MPa). b) Stress versus time. c) Effect of temperature on initial stiffness (k), bulk modulus (K, estimated using k and the shear storage modulus from DMTA), and volumetric compression set. The dashed lines are Arrhenius fits.

cycle, the trend can be fitted with a power law. A similar pronounced step in the hysteresis loss was reported in Refs. [21–24]. The U_{rel} value (Fig. 9d) also has a pronounced reduction from the 1st to the 2nd cycle, and from the 2nd to the 8th cycle it decreases further, but less than U does.

4.2.5. *Effect of strain amplitude*

Fig. 7a (100 °C) and Fig. 7b (23 °C) show how the strain amplitude affects the non-linearity of the stress-strain curve for the first loading and unloading. At 100 °C, the material is softer, so the derivative of the stress-strain curve is lower during loading (Fig. 7c). At large strains, also the second derivative is lower at 100 °C. During unloading at 100 °C there is a distinct change in slope for the derivative around 68% strain (Fig. 7c). This was not observed when unloading from 50% strain at 100 °C, or when unloading from 70% strain at 23 °C. The distinct change in slope for the derivative could be related to a change in the micro-mechanics. A parallel could be drawn to Ref. [41], which developed a material model for the Mullins effect and cyclic softening of a filled elastomer. The model combined hyperelasticity and internal sliding with friction. During both loading and unloading there was an onset of sliding at a certain criterion. The onset of sliding during unloading gave a curve with a change of slope similar to our data. Furthermore, if we assume a mechanism as in Ref. [41] to be active in our TPV, this indicates that the onset occurs at a lower strain at 100 °C than at 23 °C.

4.3. *A model for the deformation mechanism of a TPV in compression*

Here, we shall attempt to explain the effect of temperature on the macro behaviour via the properties of the individual phases in the TPV, by including temperature effects in a micromechanics model suggested for TPVs [33].

Soliman et al. [33] proposed a deformation mechanism for a TPV-(EPDM + PP), considering a single elastomer sphere coated with a layer of thermoplastic, see Fig. 13a. In-situ infrared spectroscopy during testing showed localized strain in the TP [33]. Upon loading, the thermoplastic around the equator is stretched above the yield stress, and the unloading causes buckling of the deformed ligaments, see Fig. 13a [33, 42]. This model has been applied to tensile loading and unloading of various TPVs [6,14,42–44]. An attempt to consider the model for compression is shown in Fig. 13b: Compression flattens the elastomeric core and deforms the thermoplastic shell, which to a certain degree resists the reshaping. Upon unloading, the adhesion between the two phases will pull the thermoplastic back.

4.3.1. *Effect of temperature on the elastomeric and thermoplastic phases*

The generic effects of temperature on the mechanical properties of elastomer and thermoplastic are summarized in Table 2: The elastomer is rather unaffected by temperature when it is above T_g, and its Poisson's ratio is close to 0.5. A typical thermoplastic has a strong temperature dependence. The modulus and yield stress decrease with increasing temperature [20,38], and the stress relaxation rate decreases with

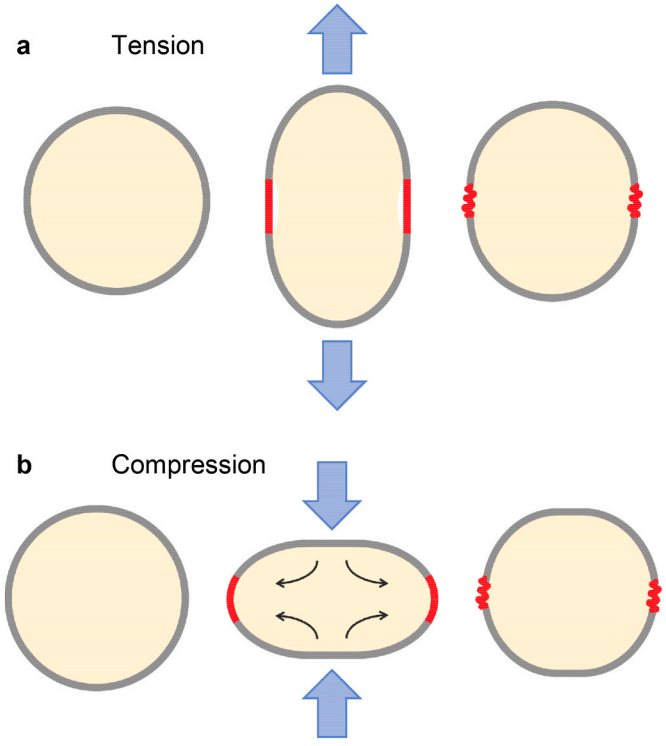

Fig. 13. Simplified behaviour of a TPV in a) tension (adapted from Ref. [33]) and b) compression. The TPV is represented by a single elastomer particle (yellow) coated with a thermoplastic layer (grey). Red indicates yielding and plastic deformation of the thermoplastic. (For interpretation of the references to colour in this figure legend, the reader is referred to the Web version of this article.)

Table 2
Simplified summary of effects of temperature on the mechanical properties of the two main phases in a TPV, in a temperature range above and below room temperature, corresponding to the service temperature range for the TPV.

	Elastomer	Thermoplastic
Modulus	Small effect of T	Decreases with increasing T
Strain recovery	Small effect of T	Small effect of T
Stress relaxation rate	Small decrease with increasing T	Decreases with increasing T Larger effect of T below T_g

increasing temperature (in the range 23–100 °C) [38]. The glass transition of the thermoplastic influences some temperature dependencies. For instance, the effect of temperature on the relaxation rate is stronger below T_g [45,46]. The Poisson's ratio of a thermoplastic is around 0.4 at 23 °C and it increases with increasing temperature [47].

Spieckermann [48] reported that for cyclic compression of a PP, the strain recovery was nearly unaffected by temperature between −20 °C and 50 °C, but the recovery was slightly lower at −20 °C for true strains above 20%. A similar absence of effect of temperature on strain recovery was reported by Drozdov and Dusunceli [20], for a PP subjected to cyclic tensile loading to 15% strain, in the temperature range 23 °C and 100 °C.

4.3.2. *Effect of temperature on the deformation mechanism*

When reducing the temperature below 23 °C, the difference in modulus between the two phases increases. Hence, when unloading below 23 °C, the elastomer-driven recovery is partially opposed by the (stiffer) thermoplastic. There is also a mismatch in Poisson's ratio (which increases with decreasing temperature) that may contribute to a multiaxial stress state in the thermoplastic. As mentioned, the stress relaxation rate of the thermoplastic increases with decreasing temperature below 23 °C. In addition, the viscoelastic recovery rate of the elastomer decreases. These factors can explain the increase in the CCS value with decreasing temperature below 23 °C (Fig. 8b).

At 23 °C and above, the stiffnesses of the thermoplastic and elastomer phases are more similar, and the elastomer may readily pull the thermoplastic back to its the original shape. The almost negligible effect of temperature on the CCS value can be attributed to the similar effect on stress relaxation. (Fig. 8b). Additionally, above a certain temperature, the elastomer may eventually be stiffer than the thermoplastic. Above this "turning point" the recoverability of the elastomer will overshadow the influence of the thermoplastic. DMTA data for an EPDM rubber (Fig. 4) suggests there is such a "turning point". (Since we have not tested the elastomeric phase in our TPV separately, the G′ of an EPDM is included in Fig. 4 to demonstrate typical properties of a crosslinked elastomer.)

The temperature dependent deformation mechanisms outlined above may be a tool to better understand the effect of temperature on a TPV subjected to cyclic loading.

4.4. *Standard compression set vs. cyclic compression set*

This sub-section will attempt to explain why the standard compression set (CS) after three weeks is higher than the cyclic compression set (CCS) at temperatures in the range 23–100 °C, but lower at −10 °C.

For compression set measurements in general, with any setting duration, the effect of temperature on the compression set may be related to 1) the kinetics of changes in links in the strained network; loss of links (e.g. via chain disentanglement, irreversible damage of the microstructure during loading or chain scission), as well as formation of new links that resist recovery (e.g. via chain entanglement, chemical crosslinking or crystallization), 2) the kinetics of strain recovery after unloading, and 3) the temperature dependence of the modulus and recovery force of the entropy-governed elastic network.

The standard CS test (ISO 815–1, method A) differs from our CCS measurements: For the CS test, the duration of compression is much longer, and the compression strain is constant. Also, the time for recovery (before measuring the residual strain) is longer (30 min). Furthermore, the entire CCS test is performed at the test temperature, while in the CS test the specimen is compressed and decompressed at room temperature, and the CS value is based on specimen heights measured at room temperature, before and after the test. This will have some consequences: 1) For tests at temperatures below the T_g of one of the phases, the deformation mechanism and potential damage will be different for the CS and CCS tests. 2) For CS tests above/below room temperature, the heating/cooling of the compressed specimen will cause a thermal stress which slightly increases/reduces the initial compressive stress in the test.

The CS value increases with increasing test time, and then seems to reach a plateau (Fig. 11a). At 100 °C, the plateau is reached when the test time is about 500 h (three weeks). In the range 23–100 °C, the CS plateau value is larger than the CCS value (after 8 cycles, as well as the power law plateau value). However, for a short CS test time, the CS value would be equal to the CCS value. For TPEs tested at 23 °C, this crossover test time can be on the order of 1–3 days [32]. Note that the CS value of a TPV will not necessarily stabilize on a plateau, even after several months. In Ref. [15], six different TPVs were tested up to 1450 h at 125 °C, but only one of them reached a plateau in this timeframe. For longer test durations than in our study, the CS value of our TPV may also increase further, above the apparent plateau.

Our 508 h CS data in the range −10 °C–100 °C shows a monotonic increase with increasing temperature (Fig. 11b). This trend is well known from technical documentation of commercial materials, and in the scientific literature it is reported for a few TPEs [49,50], and for several rubbers [51,52]. It can be related to long-term physical and/or chemical processes that affect the network [53–55].

In the range 23 °C–100 °C, the CS value is larger than the CCS value (and the difference increases with increasing temperature), but at −10 °C it is opposite (Figs. 8b and 11c). Hence, the difference (CS - CCS) increases in the entire temperature range (being negative at −10 °C). The CS value being higher than the CCS value is due to the long duration of the CS test, and the physical and chemical processes mentioned above. The opposite observation at −10 °C is due to the difference between the two tests (see above). One possible reason is that in the CS test the specimen is loaded and unloaded at room temperature, while in the CCS test this occurs at the test temperature. Hence, for tests at −10 °C, the loading in the CCS test will cause more plastic deformation and damage in the PP phase. Furthermore, the CCS test allows less recovery due to shorter recovery time and lower recovery temperature. The PP phase, in particular, will resist the recovery at low temperatures, due to its increased stiffness relative to the elastomer stiffness at low temperatures. Similar arguments can be used to explain that the difference (CS - CCS) increases with temperature in the entire temperature range.

4.5. *Poisson's ratio*

The Poisson's ratio was determined via two methods: (i) Directly from uniaxial transverse strain vs axial strain in uniaxial compression using DIC (using Eq. (1)). (ii) Indirectly, from a combination of triaxial compression and DMTA (using Eq. (10)).

The first method allowed for determining the Poisson's ratio in the entire strain range, but the method is sensitive to inhomogeneities in the strain field (especially for small strains). Poisson's ratios determined by this method exceeded 0.5 in some cases, and the standard deviations were up to 0.04 (Fig. 10a). This is believed to be due to the low, but non-zero, friction between specimen and compression plate.

Regarding the second method, it was showed that the initial slope from the triaxial compression test (k) was a good approximation of the bulk modulus (K). The second method seemed more robust, as the Poisson's ratio was calculated from entities with good repeatability (k and G′). The sensitivity of the Poisson's ratio obtained Eq. (10) to the

variation in G and k values is low; a variation of 10% affects the Poisson's ratio by only around 0.1%. However, there could be systematic errors. One such error could be that friction in the triaxial test would give a k value in Eq. (10) which is too high, leading to a too high calculated Poisson's ratio. If we take the Poisson's ratio determined at 23 °C as an example (0.4973), the k value must have been about 24% lower to affect the third decimal of this Poisson's ratio. Hence, the friction in a lubricated triaxial test probably has a small effect on the determined Poisson's ratio. Another systematic error could be related to the anisotropy of the specimens.

5. Conclusion

The temperature dependence of the cyclic compression of a TPV has been studied. This study complements the TPV literature which has very few studies of temperature dependence, and even fewer with compressive cyclic loading.

The TPV in the study was a TPV-(xSEBS + PP) with a Tg of −55 °C (attributed to the xSEBS) and a melting temperature of 147 °C (for the PP). The study covered the temperature range −40 °C–100 °C.

The observed trends for the cyclic compression behaviour versus temperature are summarized as follows:

- The secant modulus at 25% compressive strain had a temperature dependence which was similar to that of the DMTA storage modulus.
- The non-linearity of the second loading curve decreased with increasing temperature. (The first loading curve was linear in this strain range.) The non-linearity is associated with the Mullins effect. Hence the Mullins effect decreased with increasing temperature.
- The hysteresis loss of a loading-unloading cycle decreased with increasing temperature in the entire temperature range from −40 °C to 100 °C, while the relative hysteresis loss (normalized by the area under the loading curve) had almost no temperature dependence from −10 °C to 100 °C.
- For the instant compression set after a given cycle (CCS) there were two regimes of temperature dependence. At 23 °C and above, the temperature had little effect, and we propose that this is linked with the small effect of temperature on the fraction of stress relaxed during the cycle. Below 23 °C, the CCS value increased with decreasing temperature, and we relate this to the increase in relative stress relaxation with decreasing temperature.

A micromechanical model (adapted from Suliman et al. [33]) was used to explain the observed temperature effects, relating them to the elastomeric and thermoplastic phases and their interaction during loading and unloading. We conclude that this model is useful in understanding the effect of temperature on a TPV's response during compressive loading and unloading.

The Poisson's ratio was determined with two methods. (i) Directly from the uniaxial cyclic loading using DIC and (ii) Indirectly by combining results from DMTA and triaxial compression. The second method is promising, since it uses tests with good repeatability. With this method, the Poisson's ratios were determined to be 0.490; 0.497 and 0.499 at −40 °C, 23 °C and 100 °C, respectively.

The CCS values were compared with data obtained with the standard (long-term) compression set (CS) test. The objective was to determine if and how the CCS values correlate with the CS values. The CCS and CS values had different temperature dependencies (even opposite trends between −10 °C and 23 °C), and this is related to the different timescales of the two tests; the CS test allows for long-term physical and/or chemical processes. Another factor contributing to the difference between CCS and CS values, and their trends, is the fact that in the CS test the specimen is loaded and unloaded at room temperature, while in the CCS test this occurs at the test temperature.

One inference of this study is that the low-temperature cyclic compression response of the TPV (data below room temperature in this study) is affected by the PP phase. The elastomer phase has a T_g below the studied temperature interval, but the PP probably has a T_g inside the interval (although not determined in this study). At low temperatures, the PP phase induces temperature effects via temperature-dependent deformation and damage. Another inference is that the cyclic compression set is linked with the stress relaxation in the test.

Author statement

Anna-Maria M. R. Persson: Conceptualization, investigation, writing – original draft, writing – review & editing. Einar L. Hinrichsen: Project administration, Funding acquisition. Erik Andreassen: Conceptualization, writing – review & editing, supervision.

Funding

This work was supported by the Research Council of Norway (grant numbers 237900 and 259869).

Declaration of competing interest

The authors declare that they have no known competing financial interests or personal relationships that could have appeared to influence the work reported in this paper.

Acknowledgements

The authors want to acknowledge contributions from Huiting Jin, Marius Johansen, Paul McMahon, Alaa Mourad and Britt Sommer on performing experiments.

References

[1] J.G. Drobny, Handbook of Thermoplastic Elastomers, 2 ed., Elsevier, Amsterdam, 2014, ISBN 978-0-323-22136-8, p. 464.
[2] R. Shanks, I. Kong, Thermoplastic elastomers, in: S. Louis (Ed.), Handbook of Thermoplastic Elastomers, NY Research Press, 2015, ISBN 978-1-63238-282-5, pp. 175–192.
[3] B.P. Grady, S.L. Cooper, C.G. Robertson, Thermoplastic elastomers, in: J.E. Mark, B. Erman, C.M. Roland (Eds.), The Science and Technology of Rubber, Academic Press, Boston, 2013, ISBN 978-0-12-394584-6, pp. 591–652.
[4] T.A. Osswald, Injection molding materials, in: T.A. Osswald, L.-S. Turng, P. Graham (Eds.), Injection Moulding Handbook, Carl Hanser, Munich, 2008, ISBN 978-1-56990-420-6, pp. 19–62.
[5] R.M.A. l'Abee, M. Van Duin, A.B. Spoelstra, J.G.P. Goossens, Soft Matter 8 (2010) 1758, https://doi.org/10.1039/B913458A.
[6] N. Ning, S. Li, H. Wu, H. Tian, P. Yao, G.-H. Hu, M. Tian, L. Zhang, Prog. Polym. Sci. 79 (2018) 61, https://doi.org/10.1016/j.progpolymsci.2017.11.003.
[7] N. Ning, X. Li, H. Tian, Y. Hua, H. Zuo, P. Yao, L. Zhang, Y. Wu, G.-H. Hu, M. Tian, RSC Adv. 7 (2017) 5451, https://doi.org/10.1039/c6ra24891h.
[8] H. Wu, M. Tian, L. Zhang, H. Tian, Y. Wu, N. Ning, G.-H. Hu, Polymers 8 (4) (2016) 127, https://doi.org/10.3390/polym8040127.
[9] A.E. Zaikin, A.R. Akhmetov, Russ. J. Appl. Chem. 93 (5) (2020) 757, https://doi.org/10.1134/S1070427220050171.
[10] A.E. Zaikin, A.R. Akhmetov, Russ. J. Appl. Chem. 92 (3) (2019) 339, https://doi.org/10.1134/S1070427219030030.
[11] J. Oderkerk, G. Groeninckx, Polymer 43 (8) (2002) 2219, https://doi.org/10.1016/S0032-3861(01)00816-3.
[12] Z. Wang, S. Li, W. Dongya, J. Zhao, J. Thermoplast. Compos. Mater. 31 (10) (2015) 1310, https://doi.org/10.1177/0892705713503672.
[13] D. Yuan, J. Ding, W. Mou, Y. Wang, Y. Chen, Polym. Test. 64 (2017) 200, https://doi.org/10.1016/j.polymertesting.2017.10.011.
[14] A. Burgoa, A. Arriaga, K. Zulueta, E.M. Acuña, J.M. Laza, R. Hernandez, J.L. Vilas, Mater. Today Commun. 25 (2020), 101395, https://doi.org/10.1016/j.mtcomm.2020.101395.
[15] J. Yun, R. Patel, D.C. Worley II, J. Appl. Polym. Sci. 105 (5) (2007) 2996, https://doi.org/10.1002/app.24151.
[16] R.R. Babu, N.K. Singha, A.K. Naskar, Express Polym. Lett. 2 (3) (2008) 226, https://doi.org/10.3144/expresspolymlett.2008.27.
[17] P. Dey, K. Naskar, G.B. Nando, B. Dash, S. Nair, G. Unnikrishnan, J. Appl. Polym. Sci. 131 (23) (2014) 41182, https://doi.org/10.1002/app.41182.
[18] L. Mullins, Rubber Chem. Technol. 42 (1) (1969) 339, https://doi.org/10.5254/1.3539210.
[19] J. Diani, B. Fayolle, P. Gilormini, Eur. Polym. J. 45 (3) (2009) 601, https://doi.org/10.1016/j.eurpolymj.2008.11.017.

[20] A.D. Drozdov, N. Dusunceli, J. Polym. Eng. 32 (1) (2012) 31, https://doi.org/10.1515/polyeng.2011.602.
[21] C.C. Wang, Y.-F. Zhang, Q.Q. Liu, Z.B. Wang, Int. Polym. Process. 32 (1) (2017) 11, https://doi.org/10.3139/217.3146.
[22] Q. Liu, K. Zang, Z. Zang, Z. Wang, J. Thermoplast. Compos. Mater. 31 (10) (2018) 1310, https://doi.org/10.1177/0892705717738288.
[23] A.D. Drozdov, J. Christiansen, Compos. Sci. Technol. 68 (15) (2008) 3114, https://doi.org/10.1016/j.compscitech.2008.07.008.
[24] A.D. Drozdov, J. Christiansen, Int. J. Solid Struct. 46 (11) (2009) 2298, https://doi.org/10.1016/j.ijsolstr.2009.01.015.
[25] A.D. Drozdov, J. deClaville Christiansen, Int. J. Eng. Sci. 147 (2020), 103200, https://doi.org/10.1016/j.ijengsci.2019.103200.
[26] G. Chagnon, E. Verron, L. Gornet, G. Marckmann, P. Charrier, J. Mech. Phys. Solid. 52 (7) (2004) 1627, https://doi.org/10.1016/j.jmps.2003.12.006.
[27] R.R. Babu, N.K. Singha, A.K. Naskar, Express Polym. Lett. 4 (4) (2010) 197, https://doi.org/10.3144/expresspolymlett.2010.26.
[28] P.H. Mott, J.R. Dorgan, C.M. Roland, J. Sound Vib. 312 (4) (2008), https://doi.org/10.1016/j.jsv.2008.01.026.
[29] A.-M.M.R. Persson, E. Andreassen, Polymers 14 (7) (2022), https://doi.org/10.3390/polym14071316.
[30] A.-M.M.R. Persson, E.L. Hinrichsen, E. Andreassen, Polym. Eng. Sci. 60 (7) (2020) 1642, https://doi.org/10.1002/pen.25408.
[31] N.S. Karode, A. Poudel, L. Fitzhenry, S. Matthews, P.R. Walsh, A.B. Coffey, Polym. Test. 62 (2017) 268, https://doi.org/10.1016/j.polymertesting.2017.07.006.
[32] A.-M. Persson and E. Andreassen, Uniaxial Compression Stress Relaxation and Compression Set of Thermoplastic Vulcanizate Elastomers - Unpublished Results. (2020-2021).
[33] M. Soliman, M. van Dijk, M. van Es, and V. Shulmeister. Deformation mechanism of thermoplastic vulcanizates investigated by combined FTIR - and stress-strain measurements. in *ANTEC Proceedings*. Year.: SPE, CRC Press IncDOI: ISBN: 9781566768047.
[34] Y. Wu, B. Shentu, Z. Weng, J. Appl. Polym. Sci. 134 (5) (2017) 44392, https://doi.org/10.1002/app.44392.
[35] P.R.S. Leite, B.G. Soares, A.S. Sirqueira, J. Appl. Polym. Sci. 120 (2) (2011) 981, https://doi.org/10.1002/app.33123.
[36] M.B. Alanalp, A. Durmus, Polymer 142 (2018) 267, https://doi.org/10.1016/j.polymer.2018.03.054.
[37] K. Zhang, D. Zhang, L. Su, L. Jiang, J. Jiang, G. Wu, J. Appl. Polym. Sci. 133 (36) (2016) 43902, https://doi.org/10.1002/app.43902.
[38] A.D. Drozdov, Mech. Time-Dependent Mater. 14 (4) (2010) 411, https://doi.org/10.1007/s11043-010-9118-5.
[39] M.C. Boyce, K. Kear, S. Socrate, K. Shaw, J. Mech. Phys. Solid. 49 (5) (2001) 1073, https://doi.org/10.1016/S0022-5096(00)00066-1.
[40] H. Cho, S. Mayer, E. Pöselt, M. Susoff, P.J. in 't Veld, G.C. Rutledge, M.C. Boyce, Polymer 128 (2017) 87, https://doi.org/10.1016/j.polymer.2017.08.065.
[41] S. Cantournet, R. Desmorat, J. Besson, Int. J. Solid Struct. 46 (11) (2009) 2255, https://doi.org/10.1016/j.ijsolstr.2008.12.025.
[42] M.C. Boyce, S. Socrate, K. Kear, O. Yeh, K. Shaw, J. Mech. Phys. Solid. 49 (6) (2001) 1323, https://doi.org/10.1016/S0022-5096(00)00075-2.
[43] K. Naskar, J.W.M. Noordermeer, Prog. Rubber Plast. Recycl. Technol. 21 (1) (2005) 1, https://doi.org/10.1177/147776060502100101.
[44] R.R. Babu, K. Naskar, Recent developments on thermoplastic elastomers by dynamic vulcanization, in: G. Heinrich (Ed.), Advanced Rubber Composites, Springer, Berlin, Heidelberg, 2010, ISBN 978-3-642-19504-4, pp. 219–247.
[45] F.J. Wortmann, K.V. Schulz, Polymer 36 (2) (1995) 315, https://doi.org/10.1016/0032-3861(95)91319-3.
[46] A.D. Drozdov, Mech. Res. Commun. 37 (8) (2010) 690, https://doi.org/10.1016/j.mechrescom.2010.10.004.
[47] D. Tscharnuter, M. Jerabek, Z. Major, R.W. Lang, Mech. Time-Dependent Mater. 15 (1) (2011) 15, https://doi.org/10.1007/s11043-010-9121-x.
[48] F.C. Spieckermann, H.R. Wilhem, E. Schafler, E.C. Alfantis, M.J. Zehetbauer, J. Eng. Mater. Technol. 131 (1) (2008), 011109, https://doi.org/10.1115/1.3030938.
[49] C. Slater, C. Davis, M. Strangwood, Polym. Degrad. Stabil. 96 (2011) 2139, https://doi.org/10.1016/j.polymdegradstab.2011.09.012.
[50] G.J.E. Biemond, R.J. Gaymans, J. Mater. Sci. 45 (1) (2010) 158, https://doi.org/10.1007/s10853-009-3911-z.
[51] T. Pervez, S.Z. Qamar, M.v.d. Velden, J. Elastomers Plastics 44 (3) (2012) 237, https://doi.org/10.1177/0095244311420530.
[52] A. Kömmling, M. Jaunich, M. Goral, D. Wolff, Polym. Degrad. Stabil. 179 (2020), 109278, https://doi.org/10.1016/j.polymdegradstab.2020.109278.
[53] T. Cui, Y.J. Chao, J.W. Van Zee, Int. J. Hydrogen Energy 37 (18) (2012) 13478, https://doi.org/10.1016/j.ijhydene.2012.06.098.
[54] M. Patel, S. Chinn, R.S. Maxwell, T.S. Wilson, S.A. Birdsell, Polym. Degrad. Stabil. 95 (12) (2010) 2499, https://doi.org/10.1016/j.polymdegradstab.2010.07.038.
[55] S. Ronan, T. Alshuth, S. Jerrams, N. Murphy, Mater. Des. 28 (5) (2007) 1513, https://doi.org/10.1016/j.matdes.2006.03.009.